Supplement for

Highly Enrichment of Heavy Metals in Fine Particulate Matter through Dust Aerosol Generation

This file includes 4 Tables and 17 Figures:

Supplementary Figure S10. Absolute concentrations of heavy metals in MOUDI samples.

Supplementary Figure S11. Modeling of the contributions of As in dust aerosols to atmospheric heavy metals.

Supplementary Figure S12. Modeling of the contributions of Cu in dust aerosols to atmospheric heavy metals.

Supplementary Figure S13. Modeling of the contributions of Mn in dust aerosols to atmospheric heavy metal.

Supplementary Figure S14. Modeling of the contributions of Ti in dust aerosols to atmospheric heavy metals.

Supplementary Figure S15. Modeling of the contributions of Zn in dust aerosols to atmospheric heavy metal.

Supplementary Figure S16. Backward trajectories.

Supplementary Figure S17. Averaged mass spectra of dust particle cluster.

Table S1. The weight percent of heavy metal in dust-$PM_{2.5}$, dust-PM_{10} and dust-PM_{30} are shown in SPECIATE datasets (Profile NO.41350). Here, profile numbers 453102.5, 4531010 and 4531030 were used.

	Weight percent		
Heavy metal	$PM_{2.5}$	PM_{10}	PM_{30}
V	0.014	0.015	0.012
Cr	0.011	0.013	0.013
Mn	0.096	0.103	0.056
Ni	0.004	0.004	0.008
Cu	0.035	0.05	0.044
Zn	0.039	0.045	0.042
As	0	0.002	0.002
Cd	0.008	0.004	0.003
Ba	0	0.012	0.042
Ti	0.335	0.362	0.171
Pb	0.053	0.044	0.05

Table S2. Soil properties: pH and soil texture

Soil Number	Location	pH	Soil texture
S1	Ulanqab, Inner Mongolia	7.8	silty loam
S2	Bai Yin Chagan, Inner Mongolia	7.5	sand
S3	Bai Yin Chagan, Inner Mongolia	7.7	sandy loam
S4	Hohhot, Inner Mongolia	7.7	sand
S5	Yumen East Town, Jiayuguan	8.1	loam
S6	Yinda Town, Jiayuguan	8.0	loam
S7	Xitushan, Jiayuguan	8.0	sand
S8	Yema Bay, Jiayuguan	7.7	loamy sand
S9	Pingliang City, Gansu Province	7.6	silty clay loam
S10	Alxa, Inner Mongolia	8.1	sand
S11	Alxa, Inner Mongolia	8.1	sand
S12	Alxa, Inner Mongolia	7.9	sand
S13	Bayingoleng, Xinjiang	7.9	loamy sand
S14	Fudan university, Shanghai	7.5	silty clay loam

Table S3. Mass collected in dust aerosols of $PM_{2.5}$ and PM_{10}.

EXP	S1 mass (g)	S2 mass (g)	S3 mass (g)	S4 mass (g)	S5 mass (g)	S6 mass (g)	S7 mass (g)	S8 mass (g)	S9 mass (g)	S10 mass (g)	S11 mass (g)	S12 mass (g)	S13 mass (g)	S14 mass (g)
$PM_{2.5}$-1	0.0034	0.0498	0.0271	0.0186	0.0322	0.015	0.013	0.0261	0.0257	0.0229	0.012	0.0343	0.0534	0.0751
$PM_{2.5}$-2	0.044	0.0424	0.0309	0.0228	0.0293	0.0221	0.0198	0.0341	0.0171	0.0297	0.0199	0.0388	0.0529	0.0585
$PM_{2.5}$-3	0.0368	0.021	0.0244	0.0245	0.0181	0.0149	0.0219	0.0335	0.0321	0.0375	0.0232	0.0337	0.0564	0.0859
PM_{10}-1	0.0738	0.0706	0.0521	0.0543	0.0606	0.0376	0.0591	0.081	0.0898	0.0806	0.097	0.0653	0.0903	0.0607
PM_{10}-2	0.0743	0.0765	0.0877	0.0384	0.0579	0.0255	0.0505	0.0732	0.0849	0.0749	0.126	0.0602	0.0872	0.0769
PM_{10}-3	0.0775	0.0691	0.0765	0.0282	0.0625	0.0266	0.0592	0.0765	0.089	0.0845	0.0772	0.0674	0.0922	0.0763

Table S4. Mass collected in MOUDI samples. Here, an S10 sample was used.

Sample	EXP1	EXP2	EXP3
	mass (g)	mass (g)	mass (g)
PM >10	0.0738	0.0891	0.0476
PM 5.6~10	0.0315	0.0531	0.0112
PM 3.2~5.6	0.0243	0.0381	0.0132
PM 1.8~3.2	0.0176	0.0206	0.0074
PM 1.0~1.8	0.0059	0.0102	0.0074
PM 0.56~1.0	0.0056	0.0037	0.0032

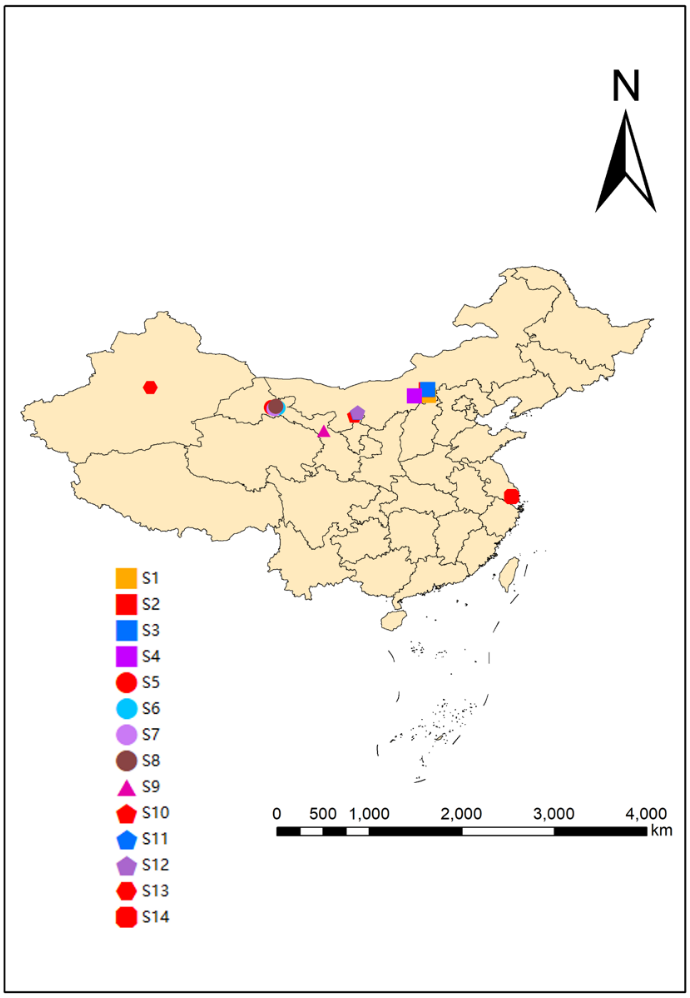

Supplementary Figure S1. Soil sampling locations. S1-S4 were collected from dust sources of the northern slope of Yinshan Mountain in central inner Mongolia and the adjacent areas of the Hunshandake Sandy Land (S1: 113.26° E, 41.01° N; S2: 113.0° E, 41.55° N; S3: 113.13° E, 41.58° N; S4: 111.85° E, 40.93° N), S5-S12 were collected from dust sources of Hexi Corridor and Alxa Plateau (S5: 97.92° E, 39.81° N; S6: 98.56° E, 39.80° N; S7: 98.20° E, 39.7° N; S8: 98.37° E, 39.94° N; S9: 103.02° E, 37.59° N; S10: 106.01° E, 39.05° N; S11: 106.31° E, 39.34° N; S12: 106.33° E, 39.37° N); S13 was collected in Xinjiang Province, in the dust sources of the Taklimakan Desert (86.15°E, 41.76°N), and S14 was sampled from Shanghai Yangpu District (121.51°E, 31.34°N).

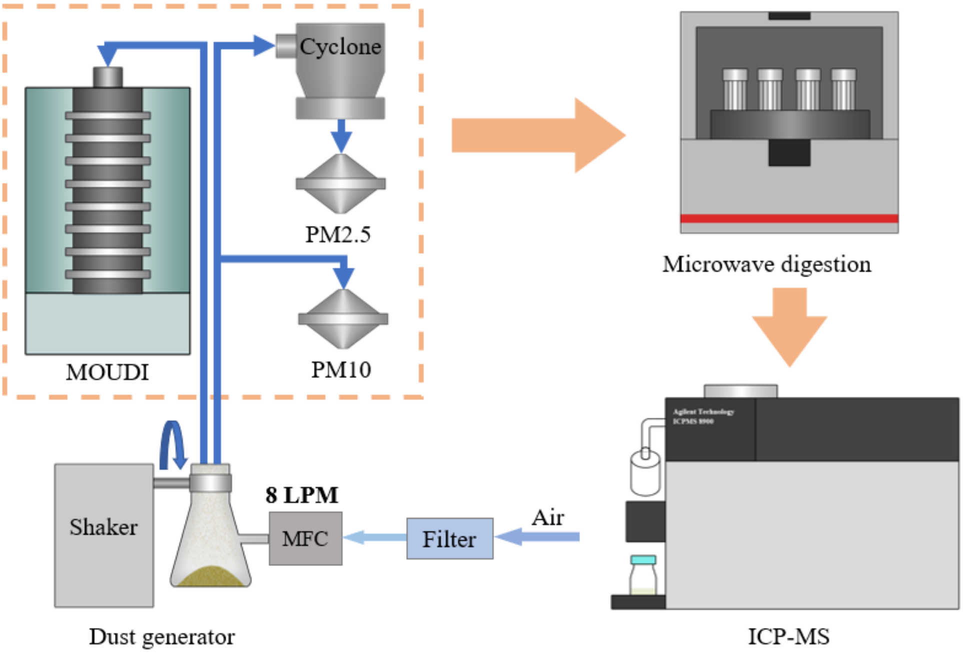

Supplementary Figure S2. Experimental setup. The setup consists of four parts: a dust generation system (Shaker), a dust particle size separation system ($PM_{2.5}$ Cyclone and MOUDI), a dust collection system (Filter holder), and the chemical analysis instrument (ICP-MS).

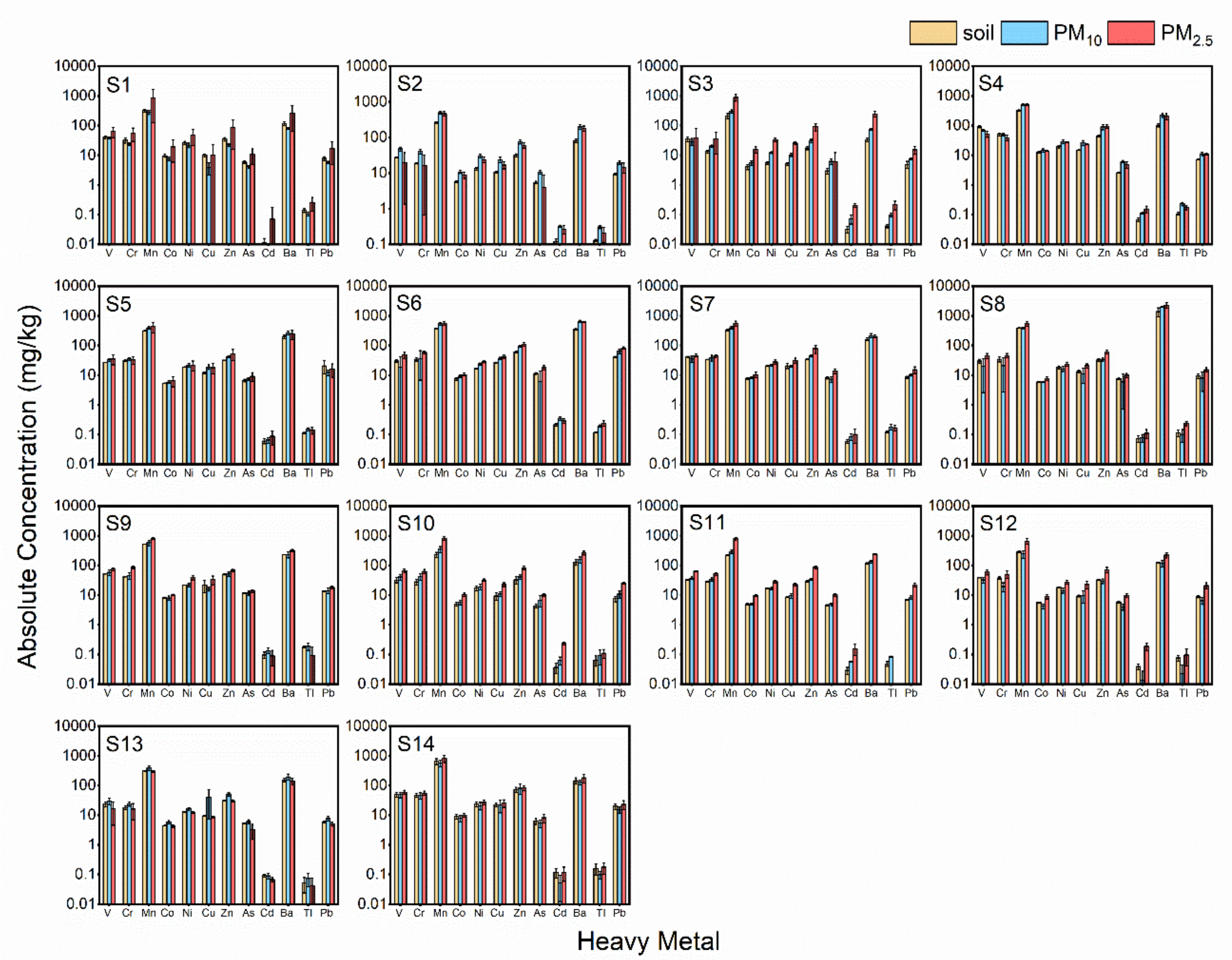

Supplementary Figure S3. Comparison of the absolute concentrations of heavy metals in the S1-S14 natural soil samples and dust aerosols. The whiskers on the bars represent the standard deviations of triplicates.

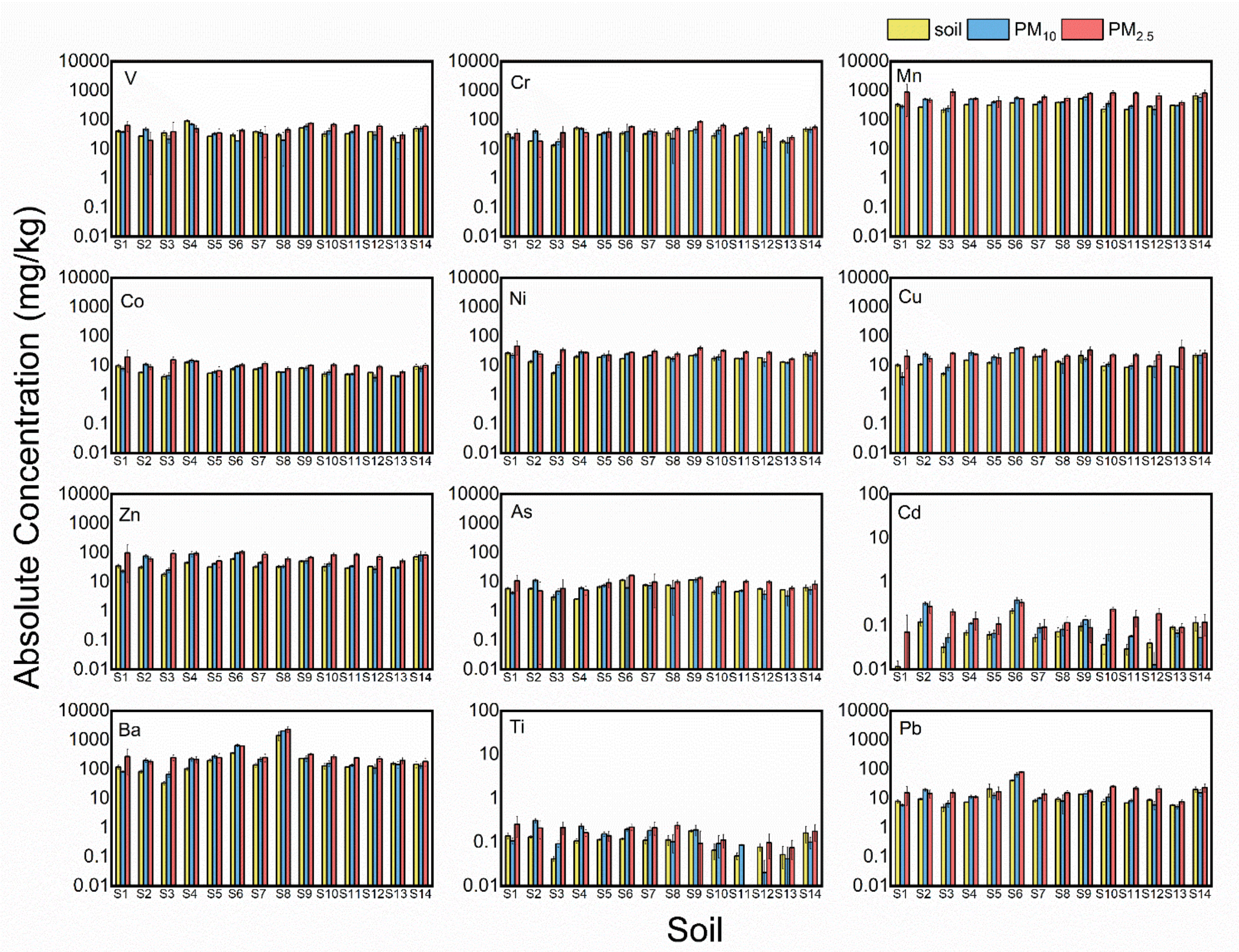

Supplementary Figure S4. Comparison of the absolute concentrations of heavy metals between natural soil samples and dust aerosols. The whiskers on the bars represent the standard deviations of triplicates.

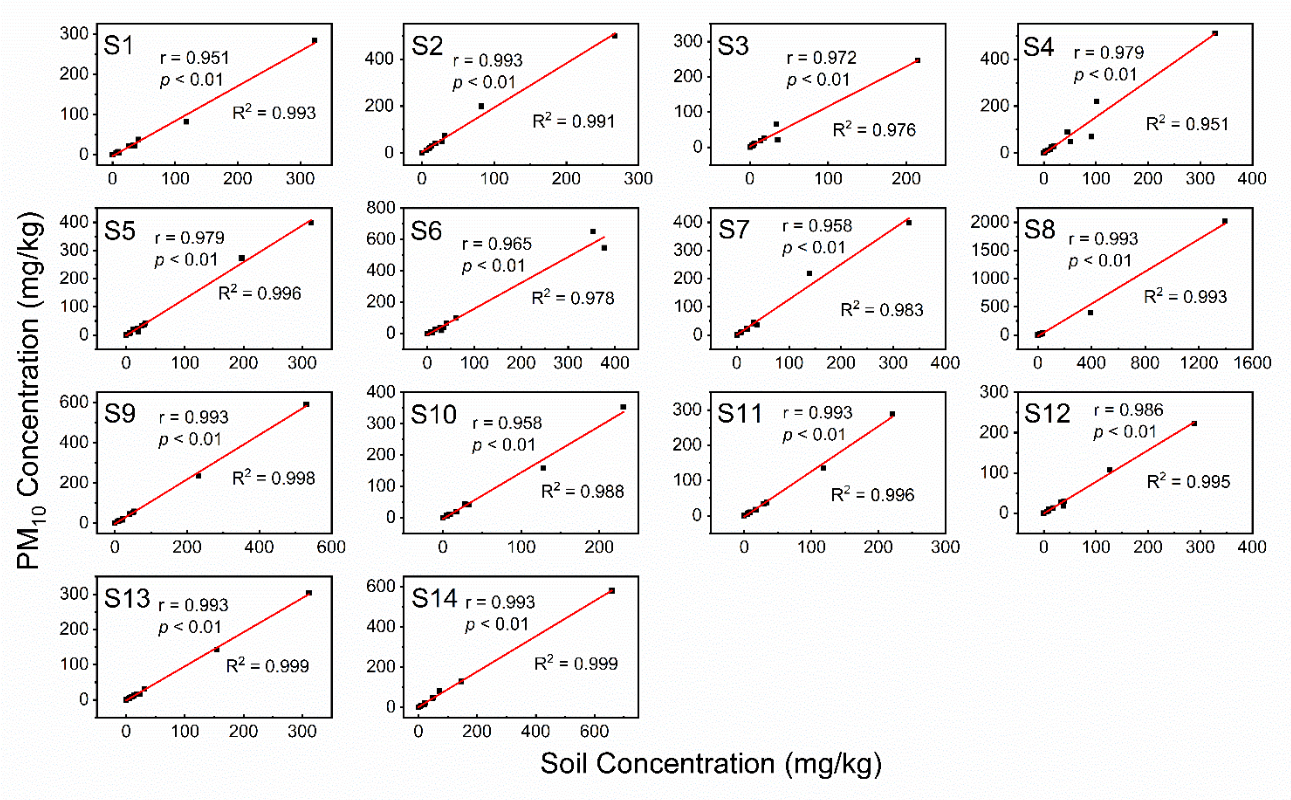

Supplementary Figure S5. Correlation between soils and PM_{10}. PM_{10} obtained by S1-S14 was compared with parent soils.

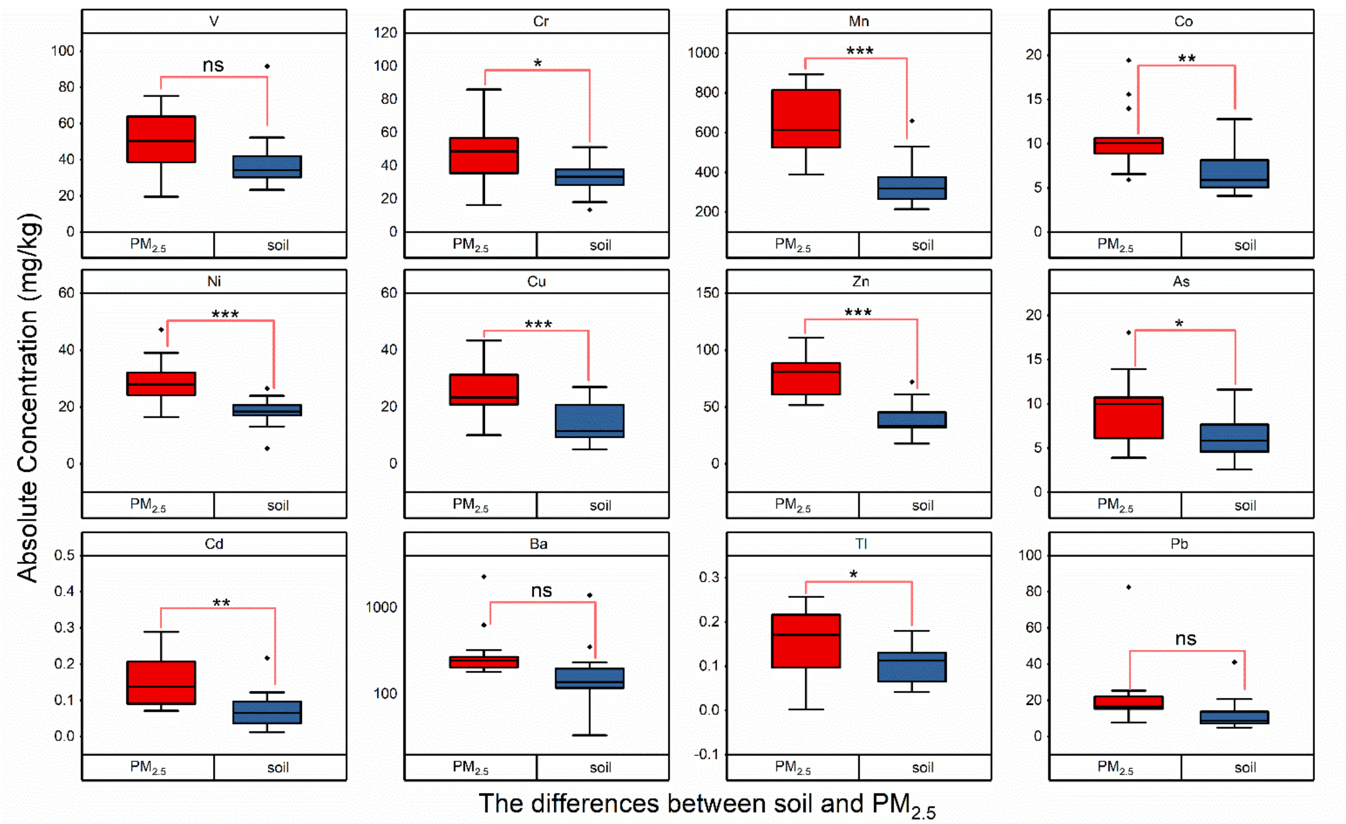

Notes: ns: not significant

∗: 0.05<p<0.01

∗∗: 0.01<p<0.001

∗∗∗: p<0.001

Supplementary Figure S6. Significance of the differences in heavy metal contents between soils and $PM_{2.5}$. Heavy metals in dust-$PM_{2.5}$ obtained by S1-S14 were compared with parent soils.

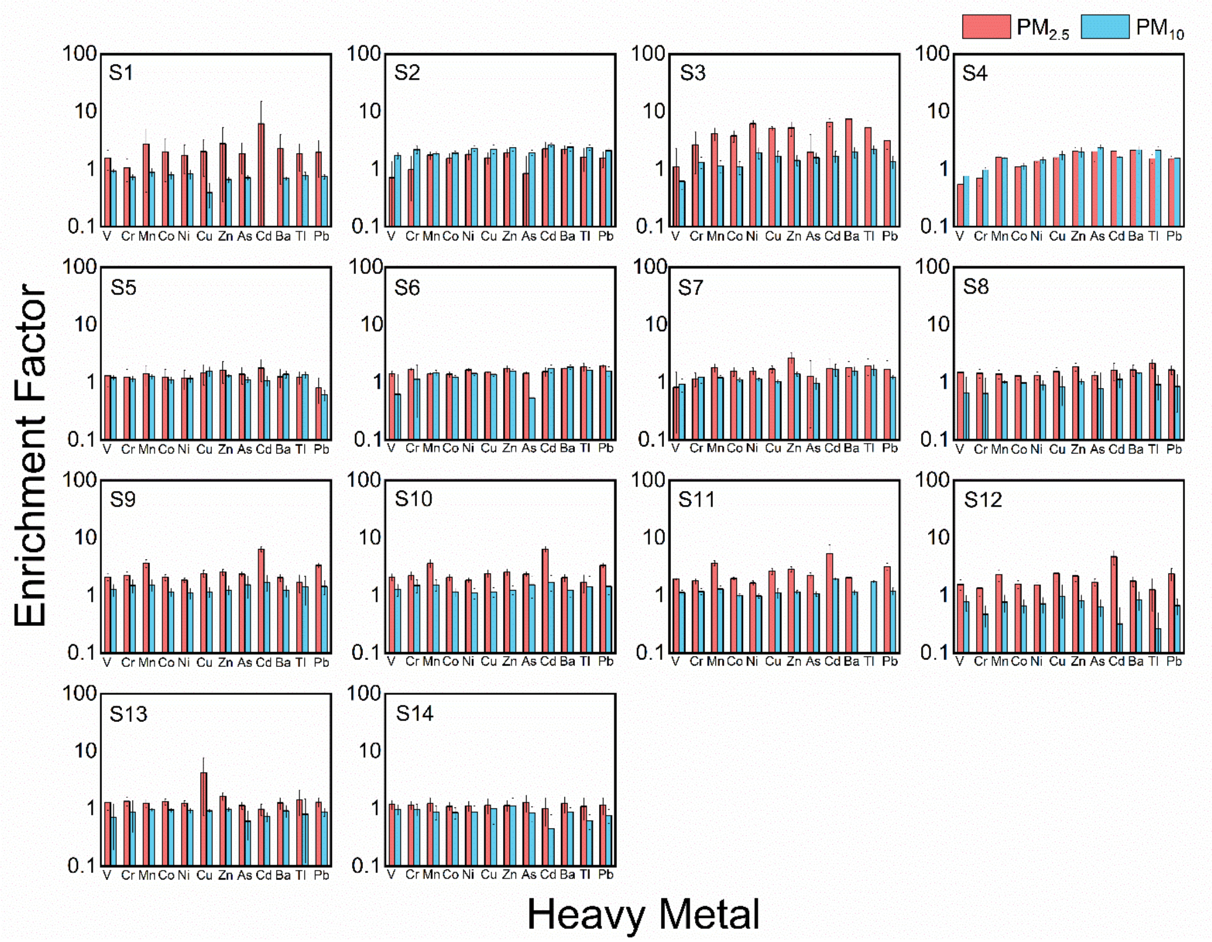

Supplementary Figure S7. Enrichment factor of heavy metals in dust-$PM_{2.5}$ and dust-PM_{10}. The whiskers on the bars represent the standard deviations of triplicates.

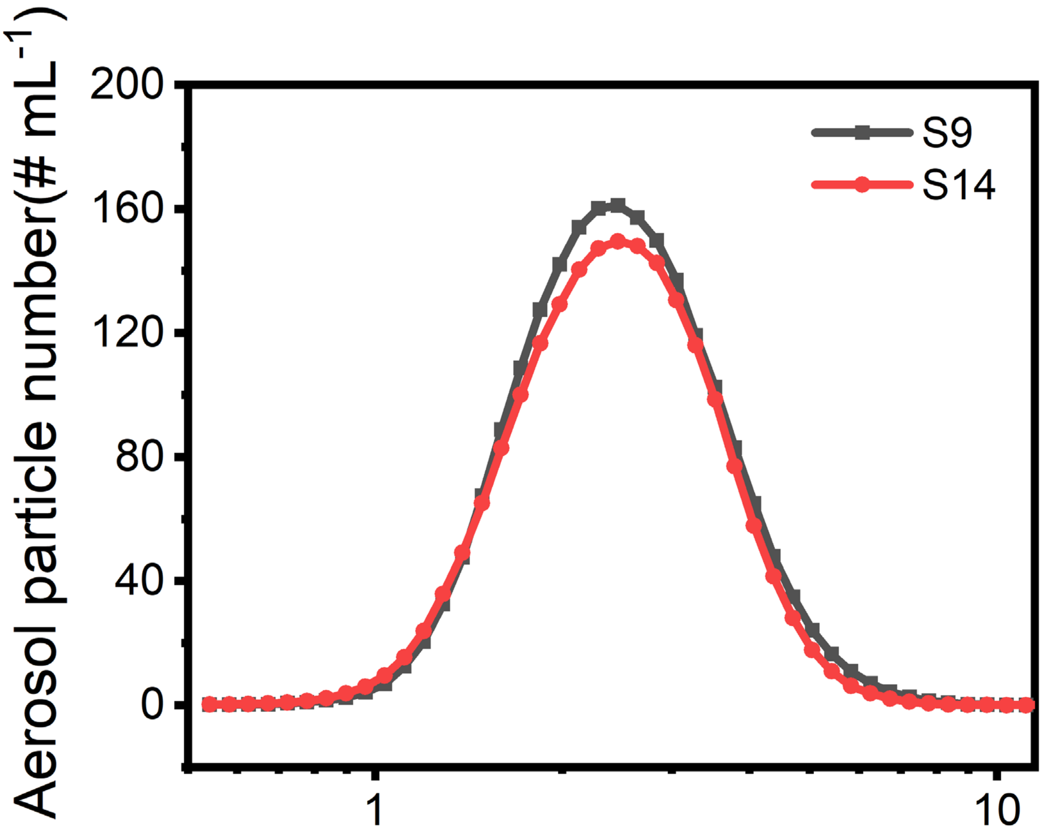

Supplementary Figure S8. Particle size distribution of dust aerosols produced from soil S9 and S14. The size distribution was detected by an Aerodynamic Particle Sizer (APS), which size range are 0.5-20 μm.

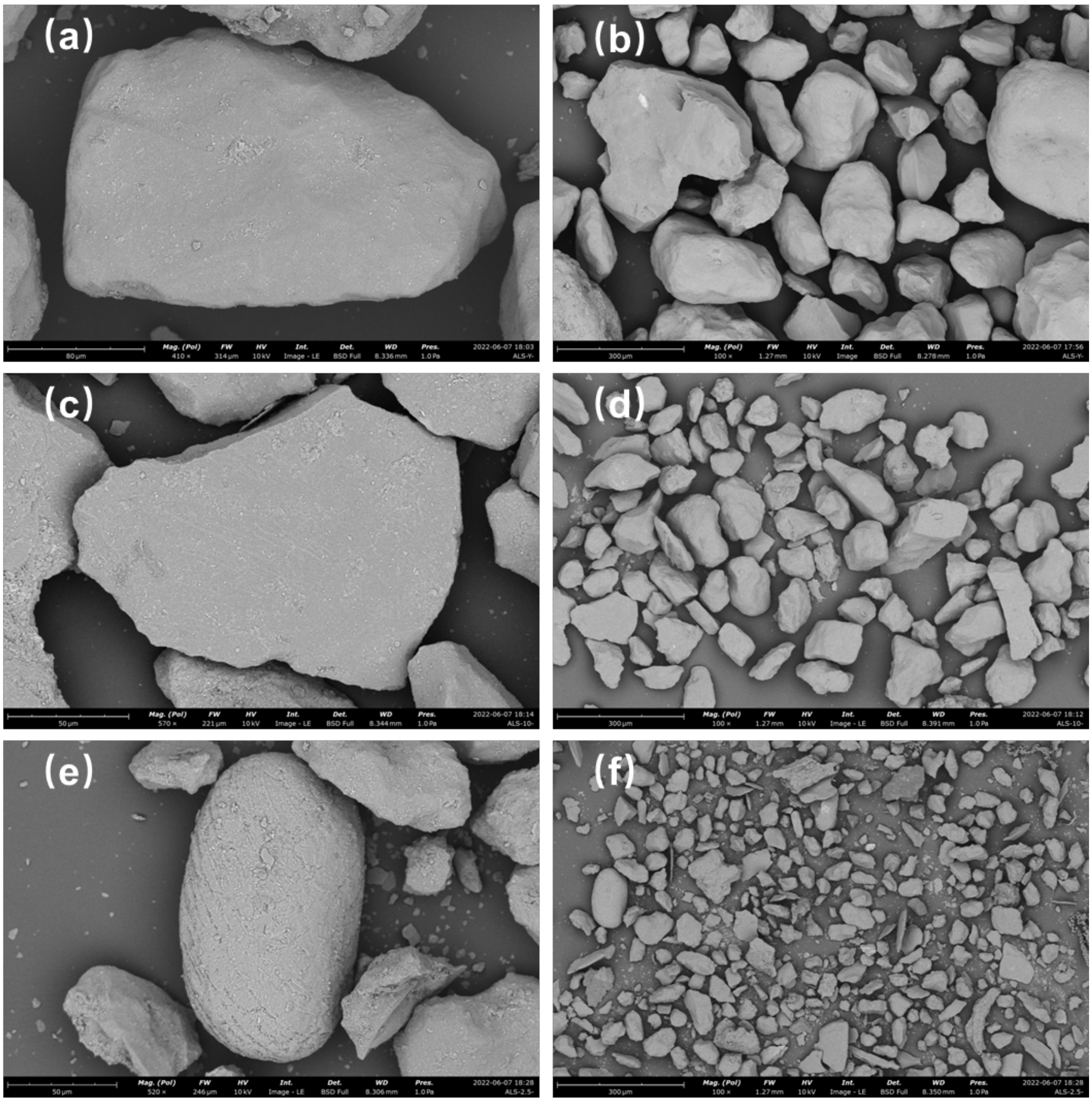

Supplementary Figure S9. SEM images of the soil and dust aerosols (generated from soil S10). (a) and (b) are natural soil images; (c) and (d) are dust-PM_{10}; and (e), (f) are dust-$PM_{2.5}$.

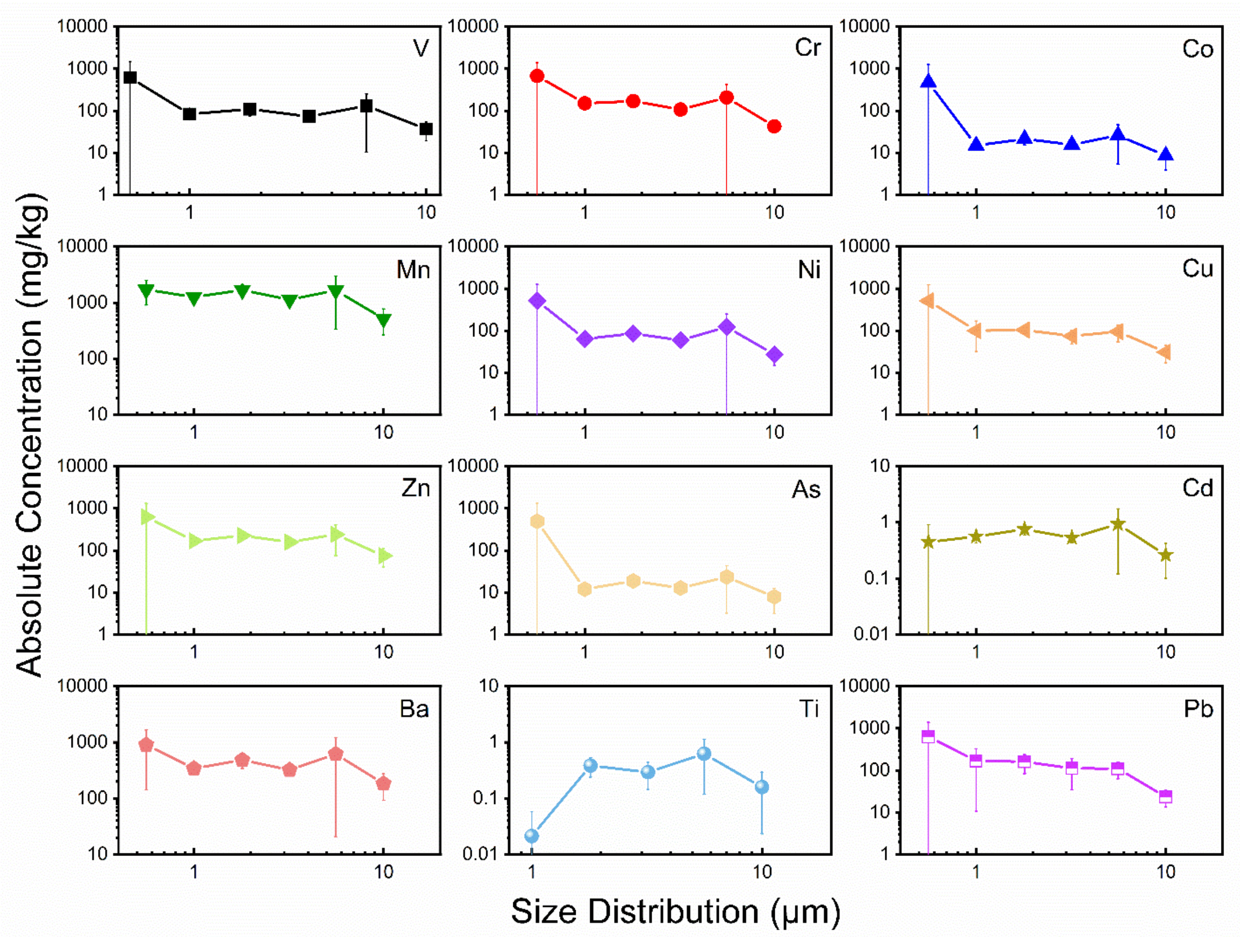

Supplementary Figure S10. Absolute concentrations of heavy metals in MOUDI samples. The particles sizes are above 10 μm, 5.6-10 μm, 3.2-5.6 μm, 1.8-3.2 μm, 1.0-1.8 μm, and 0.56-1.0 μm, respectively. Here, soil S10 was used.

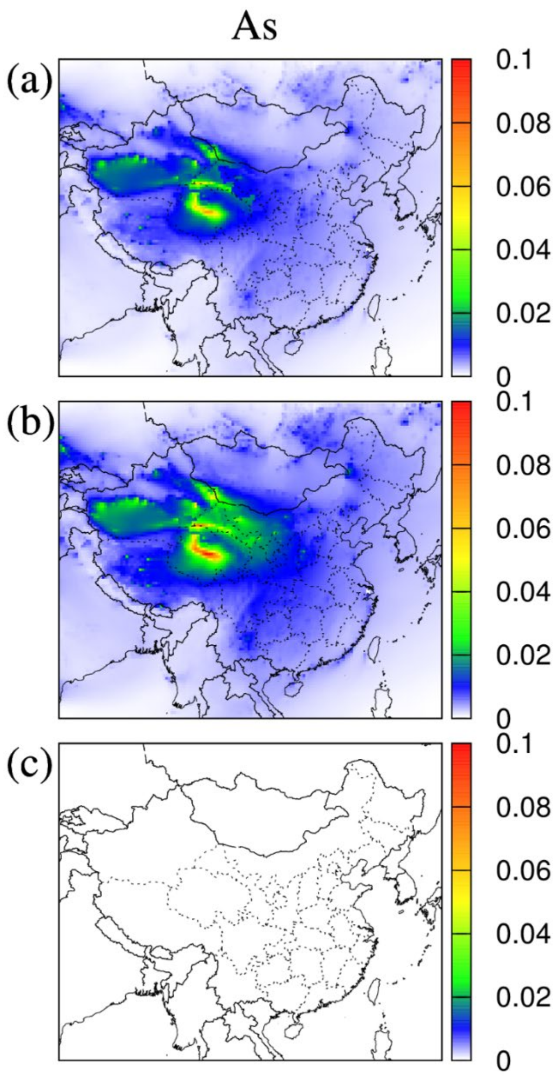

Supplementary Figure S11. Modeling of the contributions of As in dust aerosols to atmospheric heavy metals. These show the modeled results of As using the dust profiles of measured soil (a), dust-$PM_{2.5}$ (b), and the SPECIATE datasets (c). The unit is $\mu g/m^3$.

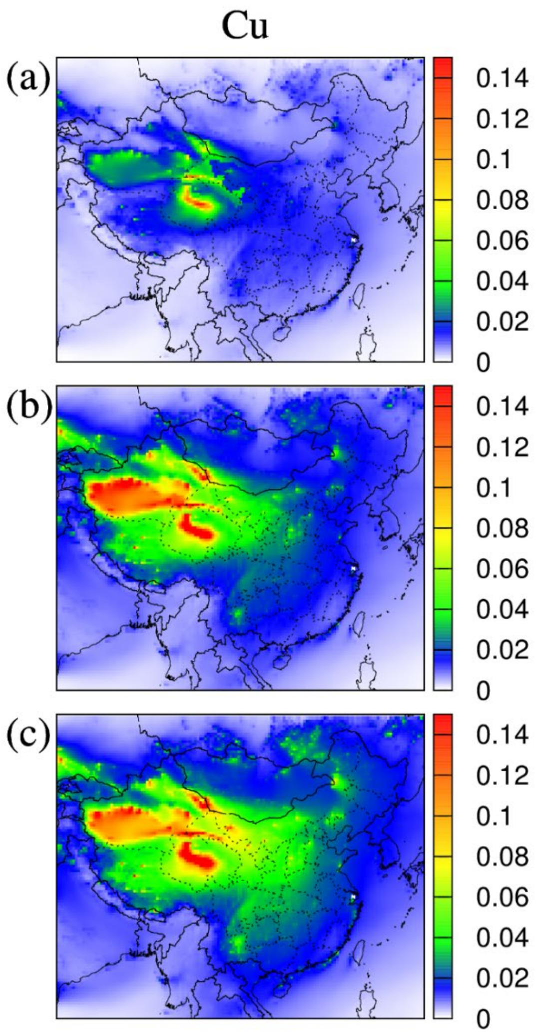

Supplementary Figure S12. Modeling of the contributions of Cu in dust aerosols to atmospheric heavy metals. These show the modeled results of Cu using the dust profiles of measured soil (a), dust-$PM_{2.5}$ (b), and the SPECIATE datasets (c). The unit is $\mu g/m^3$.

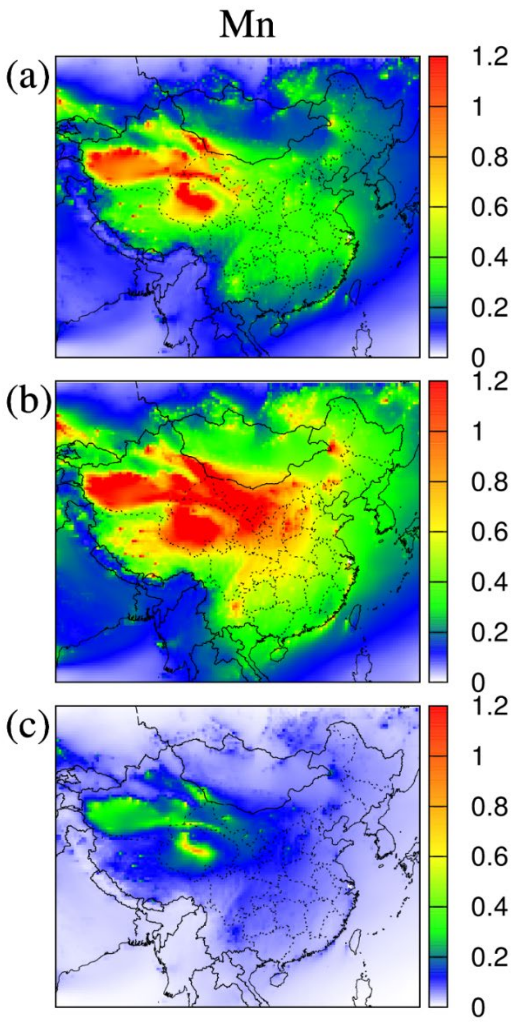

Supplementary Figure S13. Modeling of the contributions of Mn in dust aerosols to atmospheric heavy metals. These show the modeled results of Mn using the dust profiles of measured soil (a), dust-$PM_{2.5}$ (b), and the SPECIATE datasets (c). The unit is $\mu g/m^3$.

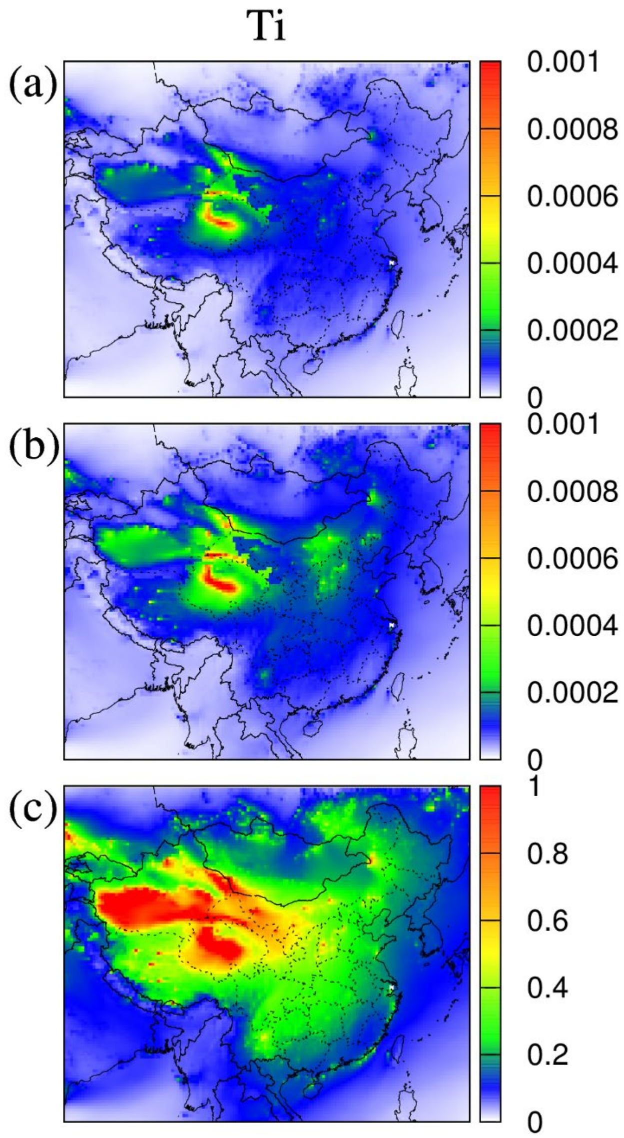

Supplementary Figure S14. Modeling of the contributions of Ti in dust aerosols to atmospheric heavy metals. These show the modeled results of Ti using the dust profiles of measured soil (a), dust-$PM_{2.5}$ (b), and the SPECIATE datasets (c). The unit is $\mu g/m^3$.

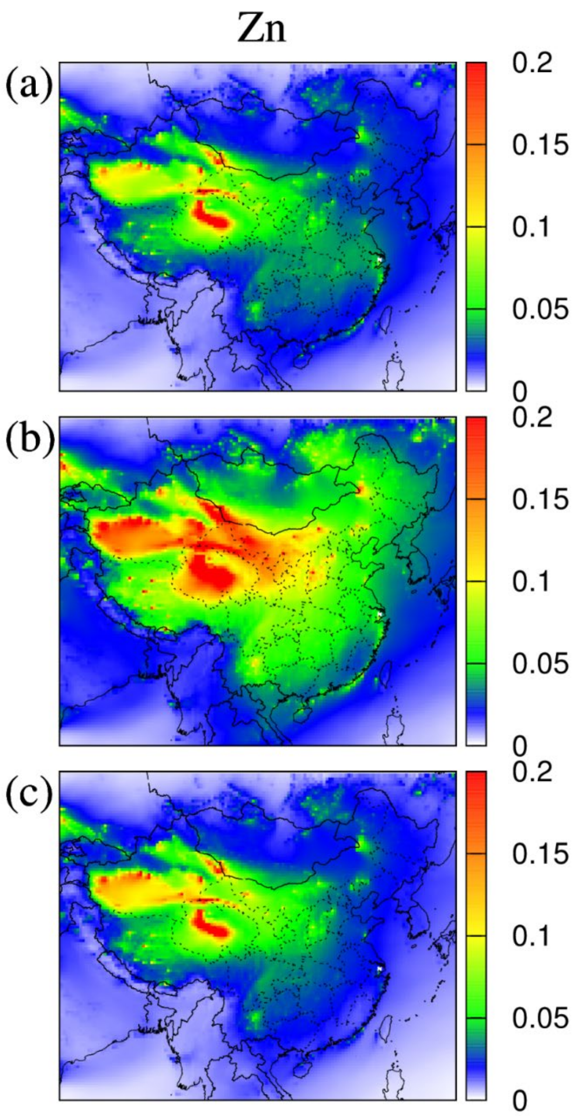

Supplementary Figure S15. Modeling of the contributions of Zn in dust aerosols to atmospheric heavy metals. These show the modeled results of Zn using the dust profiles of measured soil (a), dust-$PM_{2.5}$ (b), and the SPECIATE datasets (c). The unit is $\mu g/m^3$.

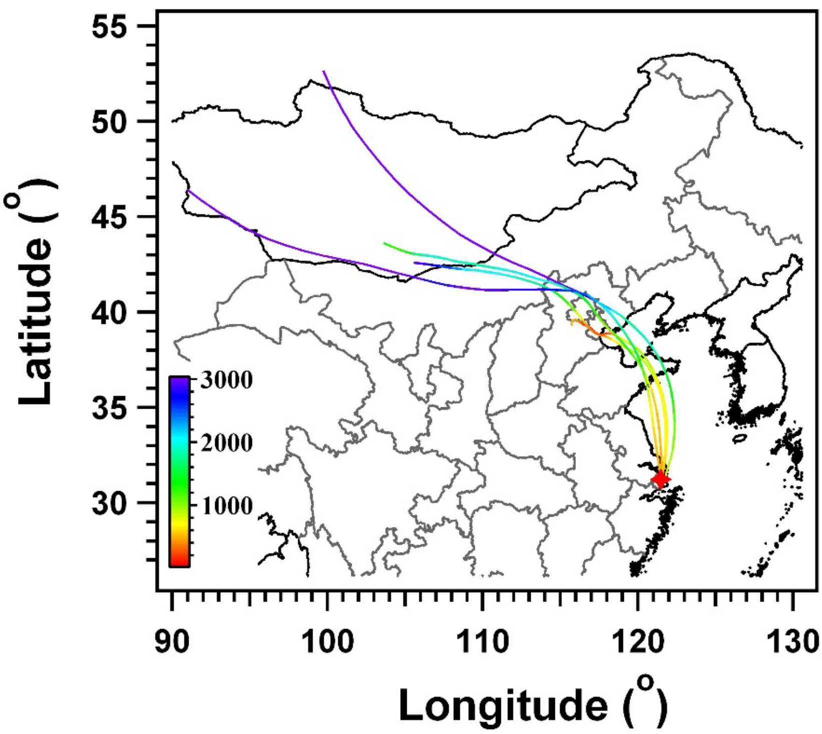

Supplementary Figure S16. Backward trajectories. The HYSPLIT 48-hour air mass backward trajectories at 500 m arrival height ending at 22:00 UTC+8 on 23 May, 2018.

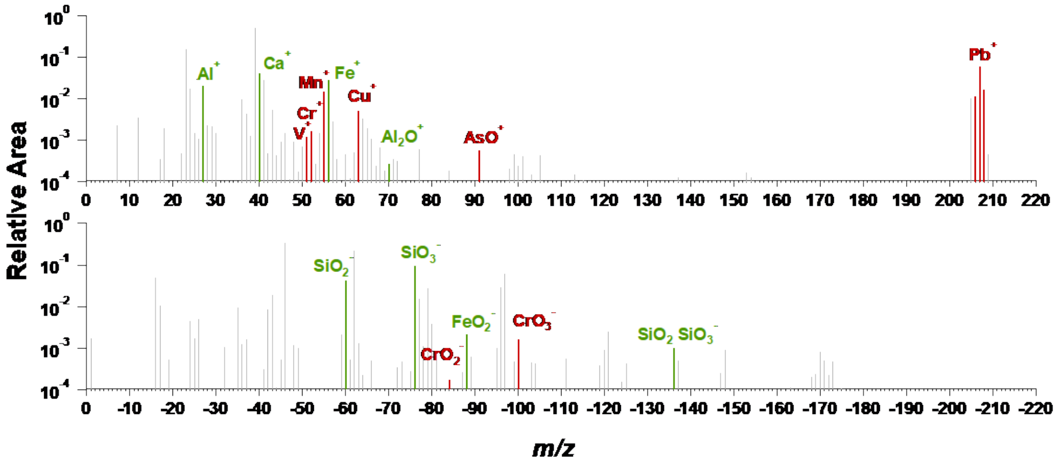

Supplementary Figure S17. Averaged mass spectra of dust particle cluster. The green sticks are typical dust markers; the red sticks are typical heavy metal markers.